

# Single Charged Higgs Boson Production in Polarized Photon Collision and the Probe of New Physics

HONG-JIAN HE<sup>1\*</sup>, SHINYA KANEMURA<sup>2†</sup>, C.-P. YUAN<sup>3‡</sup>

<sup>1</sup>*Center for Particle Physics, University of Texas at Austin, Texas 78712, USA*

<sup>2</sup>*Theory Group, KEK, Tsukuba, Ibaraki 305-0081, Japan*

<sup>3</sup>*Department of Physics and Astronomy,*

*Michigan State University, East Lansing, Michigan 48824, USA*

## Abstract

We study single charged Higgs boson production in photon-photon collision as a probe of the new dynamics of Higgs interactions. This is particularly important when the mass ( $M_{H^\pm}$ ) of charged Higgs bosons ( $H^\pm$ ) is relatively heavy and above the kinematic limit of the pair production ( $M_{H^\pm} > \sqrt{s}/2$ ). We analyze the cross sections of single charged Higgs boson production from the photon-photon fusion processes,  $\gamma\gamma \rightarrow \tau\bar{\nu}H^+$  and  $\gamma\gamma \rightarrow b\bar{c}H^+$ , as motivated by the minimal supersymmetric standard model and the dynamical Topcolor model. We find that the cross sections at such a  $\gamma\gamma$  collider can be sufficiently large even for  $M_{H^\pm} > \sqrt{s}/2$ , and is typically one to two orders of magnitude higher than that at its parent  $e^-e^+$  collider. We further demonstrate that the polarized photon beams can provide an important means to determine the chirality structure of Higgs Yukawa interactions with the fermions.

PACS numbers: 12.60.-i, 12.15.-y, 11.15.Ex

[ September, 2002 ]

---

\* [hjhe@physics.utexas.edu](mailto:hjhe@physics.utexas.edu)

† [shinya.kanemura@kek.jp](mailto:shinya.kanemura@kek.jp)

‡ [yuan@pa.msu.edu](mailto:yuan@pa.msu.edu)

## I. INTRODUCTION

The Standard Model (SM) of particle physics demands a single neutral physical Higgs scalar ( $h^0$ ) [1] to generate masses for all observed weak gauge bosons, quarks and leptons, while leaving the mass of Higgs boson and all its Yukawa couplings unpredicted. A charged Higgs boson ( $H^\pm$ ) is an unambiguous signature of the new physics beyond the SM. Most extensions of the SM require an extended electroweak symmetry breaking (EWSB) sector with charged Higgs scalars as part of its physical spectrum at the weak scale. The electroweak gauge interactions of  $H^\pm$  are universally determined by its electric charge and weak-isospin, while the Yukawa couplings of  $H^\pm$  are model-dependent and can initiate new production mechanisms for  $H^\pm$  at high energy colliders. Most of the underlying theories that describe the EWSB mechanism can be categorized as either a “supersymmetric” (with fundamental Higgs scalars) [2] or a “dynamical” (with composite Higgs scalars) [3] model. The minimal supersymmetric SM (MSSM) [4] and the dynamical Top-color model [5] are two typical examples. As we will show, the Yukawa couplings associated with the third family quarks and leptons can be large and distinguishable in these models, so that measuring the single charged scalar production rate in the polarized photon collisions can discriminate these models of flavor symmetry breaking.

If a charged Higgs boson could be sufficiently light, with mass ( $M_{H^\pm}$ ) below  $\sim 170$  GeV, it may be produced from the top quark decay,  $t \rightarrow H^+ b$  [6], at the hadron colliders, including the Fermilab Tevatron and the CERN Large Hadron Collider (LHC). For  $M_{H^\pm} > m_t - m_b$ ,  $H^\pm$  can be searched at the Tevatron and the LHC from the production processes  $gb \rightarrow H^\pm t$  [7],  $cs, cb \rightarrow H^\pm$  [8, 9, 10, 11], and  $gg, q\bar{q} \rightarrow H^\pm W^\mp$  [12, 13], etc. The associated production of  $H^\pm t$  from  $gb$  fusion is difficult to detect at the Tevatron because of its small rate (largely suppressed by the final state phase space), but it should be observable at the LHC for  $M_{H^\pm} \lesssim 1$  TeV. The single  $H^\pm$  production from  $cs$  or  $cb$  fusions is kinematically

advantageous so that it can yield a sizable signal rate, and can be detected at colliders as long as the relevant Yukawa couplings are not too small [8, 10]. The  $gg \rightarrow H^\pm W^\mp$  process originates from loop corrections, and is generally small for producing a heavy  $H^\pm$  unless its rate is enhanced by  $s$ -channel resonants, such as  $gg \rightarrow H^0$ (or  $A^0$ )  $\rightarrow H^\pm W^\mp$ . Similarly, the rate of  $q\bar{q} \rightarrow H^\pm W^\mp$  is small in a general two-Higgs-doublet model (2HDM). This is because for light quarks in the initial state, this process can only occur at loop level, and for heavy quarks in the initial state, this process can take place at tree level via Yukawa couplings but is suppressed by small parton luminosities of heavy quarks inside the proton (or anti-proton). If  $H^\pm$  is in a triplet representation, the  $Z$ - $H^\pm$ - $W^\mp$  vertex can arise from a custodial breaking term in the tree level Lagrangian, but its strength has to be small due to the strong experimental constraint on the  $\rho$ -parameter. Hence, the production rate of  $q\bar{q} \rightarrow Z \rightarrow H^\pm W^\mp$  cannot be large either. At hadron colliders, the charged Higgs bosons can also be produced in pairs via the  $s$ -channel  $q\bar{q}$  fusion process through the gauge interactions of  $\gamma$ - $H^+$ - $H^-$  and  $Z$ - $H^+$ - $H^-$  [14]. However, the rate of the pair production generally is much smaller than that predicted by the single charged Higgs boson production mechanisms when the mass of the charged Higgs boson increases.

If  $M_{H^\pm}$  is smaller than half of the center-of-mass energy ( $\sqrt{s}$ ) of a Linear Collider (LC), then  $H^\pm$  may be copiously produced in pairs via the scattering processes  $e^-e^+ \rightarrow H^-H^+$  and  $\gamma\gamma \rightarrow H^-H^+$  [15]. The production rate of a  $H^-H^+$  pair is determined by the electroweak gauge interactions of  $H^\pm$ , which depends only on the electric charge and weak-isospin of  $H^\pm$ . When  $M_{H^\pm} > \sqrt{s}/2$ , it is no longer possible to produce the charged Higgs bosons in pairs. In this case, the predominant production mechanism of the charged Higgs boson is via the single charged Higgs boson production processes, such as the loop induced process  $e^-e^+ \rightarrow H^\pm W^\mp$  [16, 17], and the tree level processes  $e^-e^+ \rightarrow b\bar{c}H^+$ ,  $\tau\bar{\nu}H^+$  and  $\gamma\gamma \rightarrow b\bar{c}H^+$ ,  $\tau\bar{\nu}H^+$  [18]. The production rate of the above tree level processes depends on the

Yukawa couplings of fermions with  $H^\pm$ . This makes it possible to discriminate models of flavor symmetry breaking by measuring the production rate of the single charged Higgs boson at LC. However, as to be discussed below, at  $e^+e^-$  colliders, the cross sections of the single  $H^\pm$  production processes induced by the Yukawa couplings of fermions with  $H^\pm$  are generally small because single  $H^\pm$  events are produced via  $s$ -channel processes (with a virtual photon or  $Z$  propagator). On the other hand, at  $\gamma\gamma$  colliders, the single  $H^\pm$  cross sections are enhanced by the presence of the  $t$ -channel diagrams which contain collinear poles in high energy collisions.

In this work, we systematically study single charged Higgs boson production associated with a fermion pair  $(\bar{f}'f)$  at photon colliders, i.e.,  $\gamma\gamma \rightarrow \bar{f}'fH^\pm$ , ( $\bar{f}'f = bc$ , or,  $\tau\nu$ ), based on our recent proposal in Ref. [18]. Two general classes of models will be discussed to predict the signal event rates – one is the weakly interacting models represented by the MSSM [4] and another is the dynamical symmetry breaking models represented by the Top-color (TopC) model [5]. We show that the yield of a heavy charged Higgs boson at a  $\gamma\gamma$  collider is typically one to two orders of magnitude larger than that at an  $e^-e^+$  collider. Furthermore, we demonstrate that a polarized photon collider can either enhance or suppress the single charged Higgs boson production, depending on the chirality structure of the corresponding Yukawa couplings. In the current analysis, we shall consider the center-of-mass energy of a  $\gamma\gamma$  collider to be about 80% of an  $e^-e^+$  collider.

It is well known that the main motivation for building a high-energy polarized photon collider is to determine the  $\text{CP}$  property of the neutral Higgs bosons [19, 20, 21]. In this work, we provide another motivation for having a polarized photon collider – to determine the chirality structure of the fermion Yukawa couplings with the charged Higgs boson via single charged Higgs boson production so as to discriminate the dynamics of flavor symmetry breaking.

## II. YUKAWA INTERACTIONS IN MSSM AND TOP-COLOR MODEL

For generality, we may define the charged Higgs Yukawa interaction as

$$\mathcal{L}_Y = \overline{f'} \left( Y_L^{f'f} P_L + Y_R^{f'f} P_R \right) f H^- + \text{h.c.}, \quad (1)$$

where  $f$  and  $f'$  represent up-type and down-type fermions, respectively, and  $P_{L,R}$  are the chirality projection operators  $P_{L,R} = (1 \mp \gamma_5)/2$ .

We first consider the Yukawa sector of the MSSM, which is similar to that of a Type-II 2HDM. The corresponding tree-level Yukawa couplings of fermions with  $H^\pm$  are given by

$$Y_{L(0)}^{f'f} = \frac{\sqrt{2}m_{f'}}{v} V_{ff'} \tan\beta, \quad Y_{R(0)}^{f'f} = \frac{\sqrt{2}m_f}{v} V_{ff'} \cot\beta, \quad (2)$$

where  $m_f$  ( $m_{f'}$ ) is the mass of the fermion  $f$  ( $f'$ ),  $\tan\beta = \langle H_u \rangle / \langle H_d \rangle$  is the ratio of the vacuum expectation values ( $\langle H_u \rangle$  and  $\langle H_d \rangle$ ) of two Higgs doublets with  $v = \sqrt{\langle H_u \rangle^2 + \langle H_d \rangle^2} \simeq 246$  GeV, and  $V_{ff'}$  is the relevant Cabibbo-Kobayashi-Maskawa (CKM) matrix element of the fermions  $f$  and  $f'$ . The coupling constants  $Y_{L(0)}^{f'f}$  and  $Y_{R(0)}^{f'f}$  vary as the input parameter  $\tan\beta$  changes. For instance, for the  $\bar{t}\text{-}\nu\text{-}H^-$  coupling,  $Y_{L(0)}^{\tau\nu}$  increases as  $\tan\beta$  grows, and reaches about  $0.20 - 0.51$  for  $\tan\beta = 20 - 50$ , while  $Y_{R(0)}^{\tau\nu}$  is zero because of the absence of right-handed Dirac neutrinos in the MSSM. Without losing generality, we shall choose the following typical inputs for our numerical analysis:

$$(Y_{L(0)}^{\tau\nu}, Y_{R(0)}^{\tau\nu}) = (0.3, 0), \quad \text{for } \tan\beta = 30. \quad (3)$$

The tree level  $\bar{b}\text{-}c\text{-}H^-$  coupling contains a CKM suppression factor  $V_{cb} \simeq 0.04$ , so that  $Y_{L(0)}^{bc}$  is around 0.03 for  $\tan\beta = 50$ , and  $Y_{R(0)}^{bc}$  is less than about  $2 \times 10^{-4}$  for  $\tan\beta > 2$ . However, the SUSY radiative correction can significantly enhance the tree level  $\bar{b}\text{-}c\text{-}H^-$  coupling. It was shown in Ref. [10] that the radiatively generated  $\bar{b}\text{-}c\text{-}H^-$  coupling from the stop-scharm ( $\tilde{t} - \tilde{c}$ ) mixings in the SUSY soft-breaking sector can be quite sizable. For instance, in the

minimal Type-A SUSY models, the non-diagonal scalar trilinear  $A$ -term for the up-type squarks can be written as [10]

$$A_u = \begin{pmatrix} 0 & 0 & 0 \\ 0 & 0 & x \\ 0 & y & 1 \end{pmatrix} A, \quad (4)$$

which generates a non-trivial  $4 \times 4$  squark mass-matrix among  $(\tilde{c}_L, \tilde{c}_R, \tilde{t}_L, \tilde{t}_R)$ . In  $A_u$ , the parameters  $(x, y)$  can be naturally of order 1, representing large  $\tilde{t} - \tilde{c}$  mixings that are consistent with all the known theoretical and experimental constraints [22, 23]. An exact diagonalization of this  $4 \times 4$  mass-matrix results in the following mass eigenvalues:

$$\begin{aligned} M_{\tilde{c}1,2}^2 &= \tilde{m}_0^2 \mp \frac{1}{2} |\sqrt{\omega_+} - \sqrt{\omega_-}|, \\ M_{\tilde{t}1,2}^2 &= \tilde{m}_0^2 \mp \frac{1}{2} |\sqrt{\omega_+} + \sqrt{\omega_-}|, \end{aligned} \quad (5)$$

with  $M_{\tilde{t}1} < M_{\tilde{c}1} < M_{\tilde{c}2} < M_{\tilde{t}2}$ . Here,  $\tilde{m}_0$  is a common scalar mass in the diagonal blocks of the squark mass-matrix,  $\omega_{\pm} = X_t^2 + (x\hat{A} \pm y\hat{A})^2$ ,  $X_t = \hat{A} - \mu m_t \cot \beta$  and  $\hat{A} = Av \sin \beta / \sqrt{2}$ . In the squark mass-eigenbasis, the  $\bar{b}$ - $c$ - $H^-$  coupling can be radiatively induced from the vertex corrections [scharm(stop)-sbottom-gluino loop] and the self-energy corrections [scharm(stop)-gluino loop]. In the Type-A models with  $x \neq 0$  and  $y = 0$ , including the one-loop SUSY-QCD corrections yields the pattern [10]:

$$\delta Y_L^{bc} \neq 0 \quad \text{and} \quad \delta Y_R^{bc} \simeq 0, \quad (6)$$

for a moderate to large  $\tan \beta$ . (As to be shown below, this pattern is opposite to that predicted in the dynamical Top-color model.) The coupling  $Y_L^{bc}$  is a function of the mixing parameter  $x$ , the Higgs mass  $M_{H^{\pm}}$ , the gluino mass  $M_{\tilde{g}}$  and the relevant squark masses. In Fig. 1, we show  $Y_L^{bc}$  as a function of the parameter  $x$  for a typical set of SUSY inputs,  $(m_{\tilde{g}}, \mu, \tilde{m}_0) = (300, 300, 600)$  GeV,  $A = -A_b = 1.75$  TeV, and  $\tan \beta = 50$ . In this figure, we have also included the QCD running effects for the tree-level Yukawa couplings, cf. Eq. (2). We find that the magnitude of the total coupling  $Y_L^{bc}$  can be naturally in the range

of  $0.03 - 0.07$  for a moderate to large  $\tan \beta$ . For a smaller value of  $\tan \beta$ , the coupling  $Y_L^{bc}$  decreases. For instance, for  $\tan \beta = 20$ , the value of  $Y_L^{bc}$  is about half of that shown in the Fig. 1.

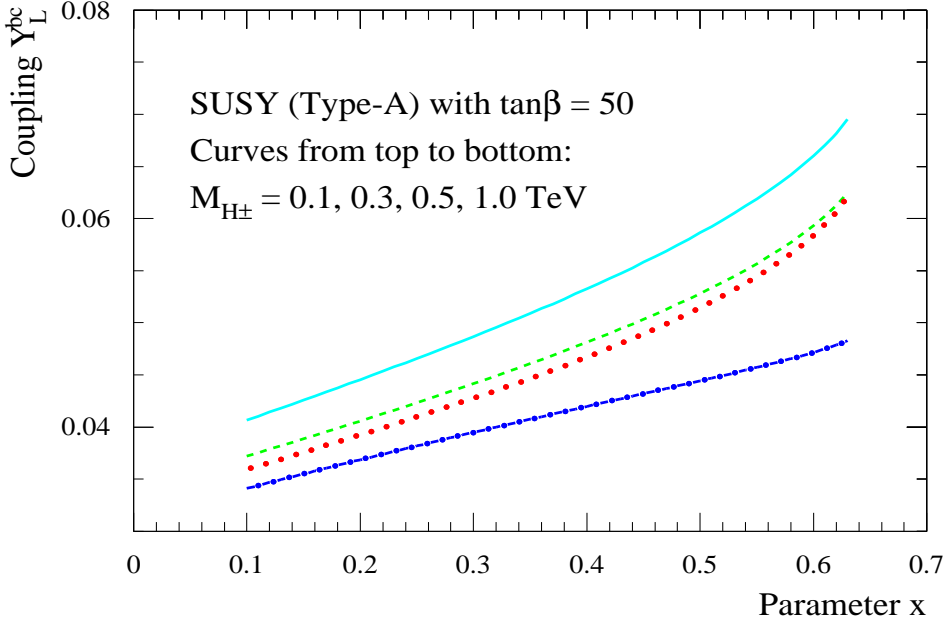


FIG. 1: The radiative  $\bar{b} \cdot c \cdot H^-$  coupling as a function of the parameter  $x$  in the minimal Type-A SUSY models with  $y = 0$ . Here, we set  $(m_{\tilde{g}}, \mu, \tilde{m}_0) = (300, 300, 600)$  GeV, and  $A = -A_b = 1.75$  TeV. This result also includes the QCD running effect for the Born level Yukawa coupling.

As discussed above, the SUSY radiative corrections are not suppressed by the small CKM matrix element  $V_{cb}$ . In addition to these, there are also corrections proportional to  $V_{cb}$ , similar to those present in the production of  $\phi^0 b\bar{b}$  ( $\phi^0 = h^0, H^0, A^0$ ) with large  $\tan \beta$  [24, 25]. This effect can be formulated by the corresponding effective Lagrangian [26],

$$\mathcal{L} = \frac{\sqrt{2} V_{cb}}{v} \frac{\overline{m}_b(\mu_R) \tan \beta}{1 + \Delta_b} H^+ \overline{c}_L b_R + \text{h.c.}, \quad (7)$$

where  $\mu_R$  is the relevant renormalization scale at which we evaluate the bottom quark running mass  $\overline{m}_b(\mu_R)$  including the NLO QCD contributions under the  $\overline{\text{MS}}$  scheme. In the

on-shell scheme, the bare mass of the bottom quark  $m_{bare}$  is equal to  $m_b + \delta m_b$ , where  $m_b$  is the pole mass and  $\delta m_b$  the counter term. A straightforward calculation shows that the threshold corrections to  $\Delta_b$  originating from the SUSY-QCD and SUSY-electroweak (SUSY-EW) contributions are equal to  $-\delta m_b/m_b$ . In general, the SUSY-EW correction comes from loop contributions induced by the Yukawa and electroweak gauge interactions, where the latter contribution is usually smaller than the former contribution. (Since in the generic Type-A model the trilinear term  $A$  needs not to be much smaller than  $\mu \tan \beta$ , we will not make the approximation  $A_b - \mu \tan \beta \approx -\mu \tan \beta$  [25] in the  $\Delta_b$  formula.) The SUSY-QCD correction is given by the finite contributions of sbottom-gluino loop due to the left-right mixings in the squark-mass matrix [26],

$$(\Delta_b)_{\text{SUSY-QCD}} = -\frac{C_F \alpha_s(\mu_R)}{2\pi} m_{\tilde{g}} M_{LR}^b \mathcal{I}(m_{\tilde{b}_1}, m_{\tilde{b}_2}, m_{\tilde{g}}), \quad (8)$$

where  $C_F = \frac{1}{2} \left( N_c - \frac{1}{N_c} \right) = \frac{4}{3}$  with  $N_c = 3$ ,  $\alpha_s \simeq 0.09$  at the scale of  $\mu_R = M_{H^\pm} = O(100) \text{ GeV}$ , and  $M_{LR}^b = A_b - \mu \tan \beta$ . The SUSY-Yukawa correction to  $\Delta_b$  arises from similar loops involving the stop and charged higgsinos  $\tilde{H}_{1,2}$ ,

$$(\Delta_b)_{\text{SUSY-Yukawa}} = +\frac{m_t^2}{8\pi^2 v^2} \frac{\mu}{\tan \beta} M_{LR}^t \mathcal{I}(m_{\tilde{t}_1}, m_{\tilde{t}_2}, \mu), \quad (9)$$

where  $y_b = \frac{\sqrt{2}m_b}{v} \tan \beta$ ,  $y_t = \frac{\sqrt{2}m_t}{v} \cot \beta$ , and  $M_{LR}^t = A_t - \mu \cot \beta$ . In the above formulas, we have defined

$$\mathcal{I}(m_1, m_2, m_3) = -\frac{m_1^2 m_2^2 \ln \frac{m_1^2}{m_2^2} + m_2^2 m_3^2 \ln \frac{m_2^2}{m_3^2} + m_3^2 m_1^2 \ln \frac{m_3^2}{m_1^2}}{(m_1^2 - m_2^2)(m_2^2 - m_3^2)(m_3^2 - m_1^2)}, \quad (10)$$

which, in the special case of  $m_1 = m_2 = m_3 \equiv M$ , equals to  $\frac{1}{2M^2}$ .

With the sample values of the SUSY-parameters given in the caption of Fig. 1,  $\Delta_b$  is found to be about 0.17, among which, 0.20 comes from the SUSY-QCD contribution, 0.00011 from SUSY-Yukawa contribution, and  $-0.022$  from the electroweak gauge contribution[32].

Hence,  $\Delta_b$  yields a factor of  $1/(1 + 0.17) \simeq 0.85$  suppression in the  $b$ - $c$ - $H^+$  coupling as compared to the QCD-improved Born level coupling (which is about 0.03 for a 300 GeV charged Higgs boson), and the coupling of  $H^+$ - $\bar{c}_L$ - $b_R$  in Eq. (7) is about 0.026 for this set of SUSY parameters. In other words, the threshold correction due to the SUSY-QCD and SUSY-EW contributions to  $Y_L^{bc}$  is  $(0.85 - 1) \times 0.03 \simeq -0.0045$ , which is not significant in the current case. (When SUSY  $\mu$  parameter flips sign, the threshold correction from  $1/(1 + \Delta_b)$  becomes an enhancement rather than suppression factor.) The additional contribution to  $Y_L^{bc}$  arising from the  $\tilde{t} - \tilde{c}$  mixing can be read out from Fig. 1 after subtracting the strength of the QCD-improved Born level coupling. For instance, using the same set of SUSY parameters described above, the radiative correction from  $\tilde{t} - \tilde{c}$  mixings with  $x = 0.44$  enhances the  $Y_L^{bc}$  coupling by an amount of 0.02 ( $\simeq 0.05 - 0.03$ ) for  $M_{H^\pm} = 300$  GeV. Therefore, the coupling of  $Y_L^{bc}$ , after including the QCD-improved Born level coupling (0.03), the radiative correction from  $\tilde{t} - \tilde{c}$  mixings (0.02), and the threshold correction due to the SUSY-QCD and SUSY-EW contributions ( $-0.0045$ ), is about 0.046 ( $\simeq 0.05$ ) for the sample SUSY parameters we have chosen. Hence, without losing generality, in the following numerical analysis, we choose

$$(Y_L^{bc}, Y_R^{bc}) = (0.05, 0) \quad (11)$$

as the sample couplings for the MSSM with natural  $\tilde{t} - \tilde{c}$  mixings, which correspond to the Type-A SUSY models with  $x = O(1)$  and  $y = 0$  as defined in Ref. [10]. (The total decay width of  $H^\pm$  will be evaluated for  $\tan\beta = 50$ .) It is worth to mention that the sample flavor-changing  $b$ - $c$ - $H^\pm$  coupling (11) is about a factor-6 smaller than the sample  $\tau$ - $\nu$ - $H^\pm$  tree-level coupling (3).

We then consider the dynamical Top-color (TopC) model [5], which is strongly motivated by the experimental fact that the observed large top quark mass ( $m_t \simeq \frac{v}{\sqrt{2}} \simeq 174$  GeV) is right at the weak scale, distinguishing the top quark from all other SM fermions. This scenario explains the top quark mass from the  $\langle \bar{t}t \rangle$  condensation via the strong  $SU(3)_{\text{tc}}$  TopC

interaction at the TeV scale. The associated strong tilting  $U(1)$  force is attractive in the  $\langle \bar{t}t \rangle$  channel and repulsive in the  $\langle \bar{b}b \rangle$  channel, so that the bottom quark mainly acquires its mass from the TopC instanton contribution [5]. This model predicts three relatively light physical top-pions ( $\pi_t^0, \pi_t^\pm$ ). The Yukawa interactions of these top-pions with the third family quarks are given by the Lagrangian,

$$\frac{m_t \tan \beta}{v} \left[ i K_{UR}^{tt} K_{UL}^{tt*} \bar{t}_L t_R \pi_t^0 + \sqrt{2} K_{UR}^{tt} K_{DL}^{bb*} \bar{b}_L t_R \pi_t^- + i K_{UR}^{tc} K_{UL}^{tt*} \bar{t}_L c_R \pi_t^0 + \sqrt{2} K_{UR}^{tc} K_{DL}^{bb*} \bar{b}_L c_R \pi_t^- + \text{h.c.} \right], \quad (12)$$

where  $\tan \beta = \sqrt{(v/v_t)^2 - 1}$  and the top-pion decay constant  $v_t \simeq O(60 - 100)$  GeV. The rotation matrices  $K_{UL,R}$  and  $K_{DL,R}$  are needed for diagonalizing the up- and down-quark mass matrices  $M_U$  and  $M_D$ , i.e.,  $K_{UL}^\dagger M_U K_{UR} = M_U^{\text{dia}}$  and  $K_{DL}^\dagger M_D K_{DR} = M_D^{\text{dia}}$ , from which the CKM matrix is defined as  $V = K_{UL}^\dagger K_{DL}$ . As shown in Ref. [8], to yield a realistic form of the CKM matrix  $V$  (such as the Wolfenstein-parametrization), the TopC model generally has the following features:

$$\begin{aligned} K_{UR}^{tt} &\simeq 0.99 - 0.94, & K_{UR}^{tc} &\lesssim 0.11 - 0.33, \\ K_{UL}^{tt} &\simeq K_{DL}^{bb} \simeq 1, \end{aligned} \quad (13)$$

which suggests that the  $t_R$ - $c_R$  transition can be naturally around 10 – 30%. Combining Eqs. (12) and (13), we can deduce the Yukawa couplings of fermions with the charged top-pion (also called charged Higgs boson throughout this paper) as

$$\begin{aligned} Y_L^{bt} &= Y_L^{bc} = 0, \\ Y_R^{bt} &\simeq \frac{\sqrt{2}m_t}{v} \tan \beta, & Y_R^{bc} &\simeq Y_R^{bt} K_{UR}^{tc}. \end{aligned} \quad (14)$$

Thus, taking a typical value of  $\tan \beta$  to be 3 and a conservative input for the  $t_R$ - $c_R$  mixing  $K_{UR}^{tc}$  to be 0.1 in the TopC model, we obtain

$$Y_R^{bt} \simeq 3, \quad \text{and} \quad (Y_L^{bc}, Y_R^{bc}) = (0, 0.3), \quad (15)$$

which will be used as the sample TopC parameters for our numerical analysis. We note that in contrast to the radiative coupling of the charged Higgs boson predicted in the Type-A SUSY model with  $y = 0$  (in which  $Y_L^{bc} \neq 0$  and  $Y_R^{bc} \simeq 0$ , i.e., mainly left-handed), the charged top-pions only have a right-handed coupling. This feature of the TopC is also opposite to the tree-level  $\tau\text{-}\nu\text{-}H^\pm$  coupling (which is purely left-handed) predicted in the MSSM [cf. Eq.(3)]. As we will demonstrate below, this feature makes it possible to discriminate the dynamical TopC model from the MSSM or a Type-II 2HDM by measuring the production rates of single charged Higgs boson at polarized photon colliders. Finally, we note that apart from the opposite chirality structures of the  $H^\pm$  Yukawa interactions, the magnitude of the sample Top-color  $b\text{-}c\text{-}H^\pm$  coupling chosen in (15) is the same as that of the sample  $\tau\text{-}\nu\text{-}H^\pm$  coupling (3).

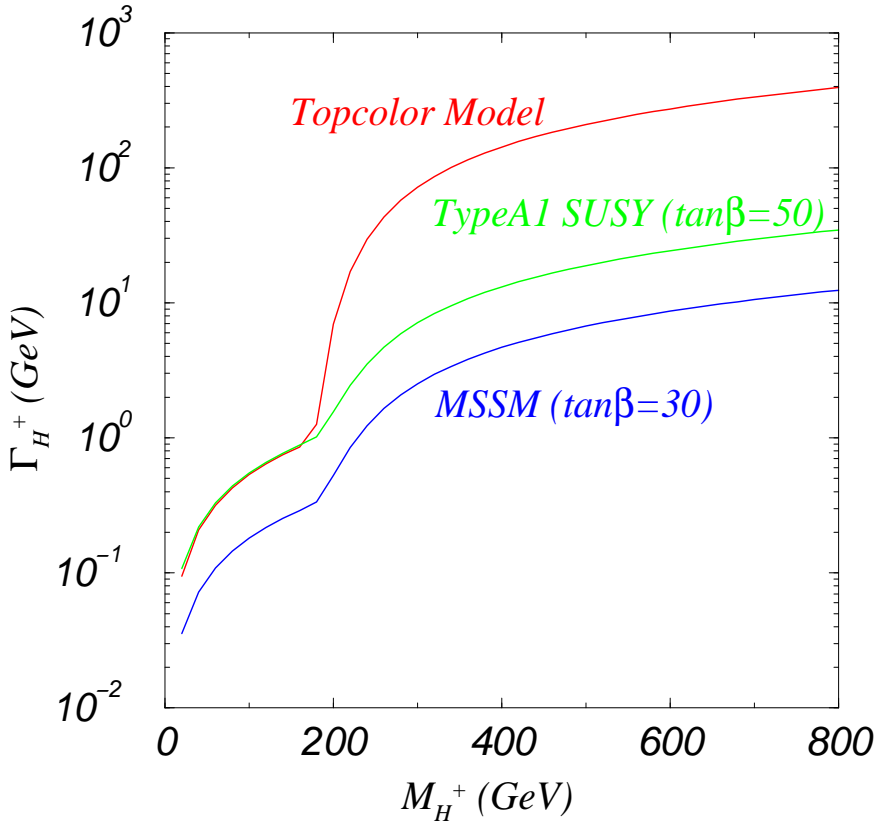


FIG. 2: The total decay widths of  $H^+$  predicted by the models discussed in the text.

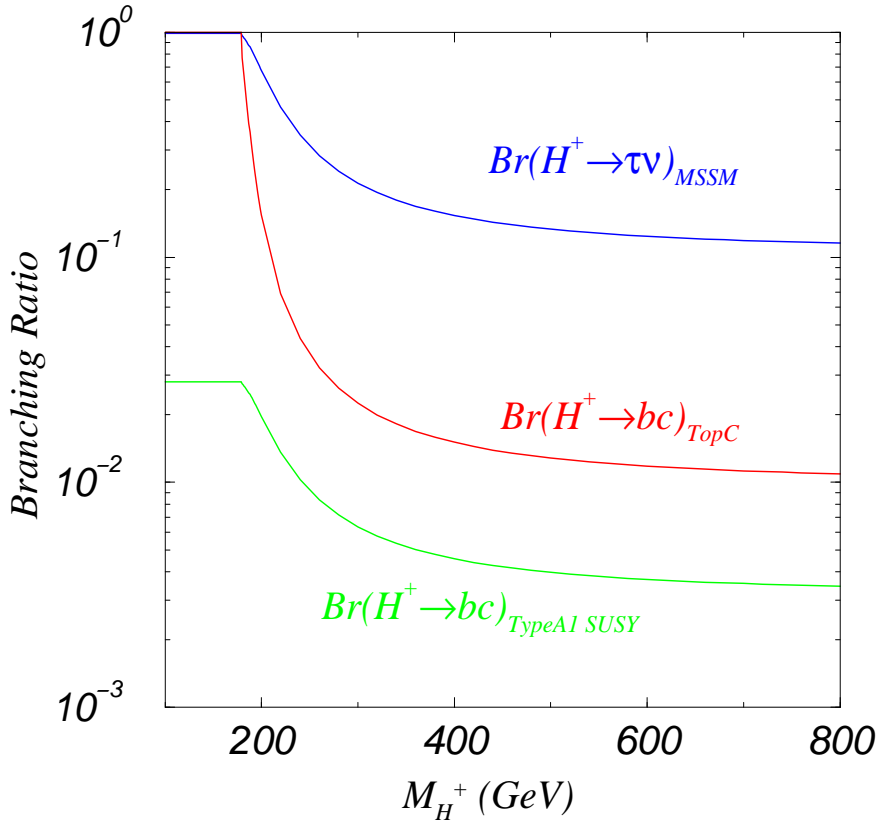


FIG. 3: The relevant decay branching ratios of  $H^+$  predicted by the models discussed in the text.

### III. $H^\pm$ PRODUCTION IN $\gamma\gamma$ COLLISION AS A PROBE OF NEW PHYSICS

We calculate the cross section of  $\gamma\gamma \rightarrow \bar{f}'f H^+$  using the helicity amplitude method for  $f'f = b\bar{c}$  or  $\tau\bar{\nu}$ . For the  $b\bar{c}$  channel, we will consider both the MSSM (with stop-scharm mixings) and the TopC model using the sample parameters listed in Eqs. (11) and (15), respectively. For the  $\tau\bar{\nu}$  channel, we will consider the MSSM with the sample parameters given in Eq. (3). The cross sections for other values of couplings, different from our sample inputs, can be deduced by a proper rescaling. In order to predict the event rate of  $\gamma\gamma \rightarrow \bar{f}'f H^+$ , we need to specify the total decay width  $\Gamma_{H^\pm}$  for  $H^\pm$ , from which the decay branching ratio of  $H^\pm \rightarrow f'f$  can be calculated. For simplicity, we shall only include the quark and lepton decay modes of  $H^\pm$  to evaluate  $\Gamma_{H^\pm}$ . Its bosonic decay modes are not included because their

contributions are generally small and strongly depend on the other parameters of the model. For example, in the MSSM, the partial decay width of  $H^\pm \rightarrow W^\pm h^0$  also depends on the neutral Higgs boson mixing angle  $\alpha$  and the light CP-even Higgs boson mass  $m_h$ . However, we find that it is generally small, especially when  $M_{H^\pm}$  becomes large which corresponds to the decoupling limit. We will also neglect all the loop-induced decay modes such as  $H^\pm \rightarrow W^\pm Z$  [27], and assume that the relevant sparticles are relatively heavy so that the SUSY decay channels of  $H^\pm$  are not kinematically accessible. Finally, in the TopC model, only the dominant  $tb$  and  $cb$  decay modes are included in the calculation of  $\Gamma_{H^+}$ . For the later analysis and discussion, we show the predicted total decay widths and the relevant decay branching ratios of  $H^+$  in Figs. 2 and 3 as the Higgs mass  $M_{H^\pm}$  varies.

In our numerical analyses, the dominant QCD corrections are included in the Yukawa couplings by using the running quark masses. For instance, at the 100 GeV scale, the running masses of the bottom and charm quarks are  $m_b = 2.9$  GeV and  $m_c = 0.6$  GeV, respectively.

### A. $b\bar{c}H^\pm$ Production

Using the default parameters of the models as described in Section II, we calculate the total cross sections of  $\gamma\gamma \rightarrow b\bar{c}H^+$  and  $e^+e^- \rightarrow b\bar{c}H^+$  as a function of  $M_{H^\pm}$ . The result for the TopC model is shown in Fig. 6, where, for comparison, we have taken the center-of-mass energy of the  $\gamma\gamma$  collider to be 0.8 times of that of the  $e^-e^+$  collider. The result for the MSSM with stop-scharm mixings can be easily obtained from Fig. 6 by rescaling the  $y$ -axis (i.e. the cross sections) by a factor of  $(0.3/0.05)^2 = 36$  when  $M_{H^\pm} > \sqrt{s}/2$ . For  $M_{H^\pm} < \sqrt{s}/2$ , where the pair production mechanism dominates, the actual rate also depends on the decay branching ratio  $\text{Br}(H^- \rightarrow b\bar{c})$  and the total decay width  $\Gamma_{H^+}$  in the MSSM. For completeness, we also show the result for the MSSM in Fig. 7, which is qualitatively similar to Fig. 6 except near the boundary of the available phase space for pair production, i.e. when

$M_{H^\pm} \sim \sqrt{s}/2$ . This is because the total decay width of  $H^\pm$  in the TopC model is much larger than that in the Type-A SUSY mode. For instance, the  $\Gamma_{H^\pm}$  of the charged Higgs boson with a mass 200 GeV (400 GeV) is about 7 GeV (143 GeV) in the TopC model [cf. Eq. (15)], and 1.5 GeV (13 GeV) in the Type-A SUSY model [cf. Eq. (11)]. The branching ratios for the decay mode  $H^\pm \rightarrow c\bar{c}$  predicted in these two models are 0.15 (0.015) and 0.02 (0.0046), respectively.

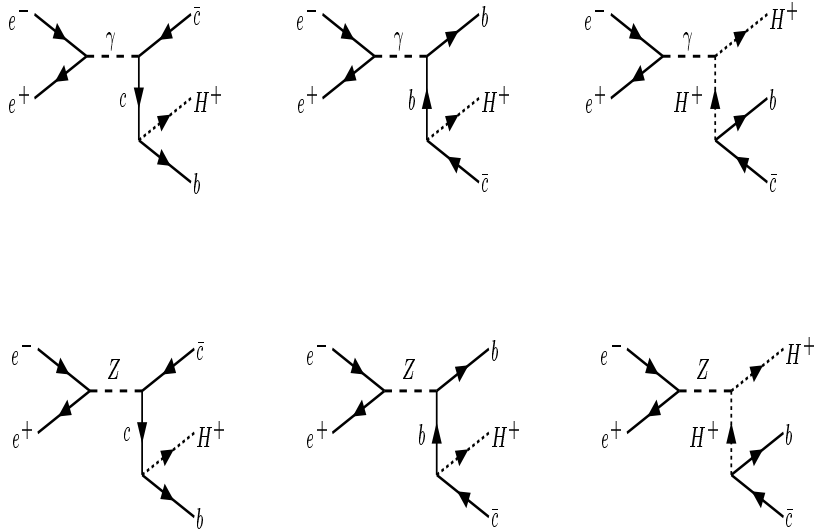


FIG. 4: The complete set of Feynman diagrams for  $e^- e^+ \rightarrow b\bar{c}H^+$ .

A few discussions on the feature of the results shown in Fig. 6 are in order. (The same discussions also apply to Fig. 7.) For  $M_{H^\pm} < \sqrt{s}/2$ , the charged Higgs pair production is kinematically allowed. In this case, the production cross section for  $\gamma\gamma \rightarrow b\bar{c}H^+$  (and  $e^- e^+ \rightarrow b\bar{c}H^+$ ) is dominated by the contribution from the pair production diagrams with the produced  $H^\pm$  decaying into a  $b\bar{c}$  pair. Hence, its rate is proportional to the decay branching ratio  $\text{Br}(H^\pm \rightarrow b\bar{c})$ . As shown in the figure, there is a *kink* structure when  $M_{H^\pm}$  is around 180 GeV. That is caused by the change in  $\text{Br}(H^\pm \rightarrow b\bar{c})$  when the decay channel  $H^\pm \rightarrow b\bar{t}$

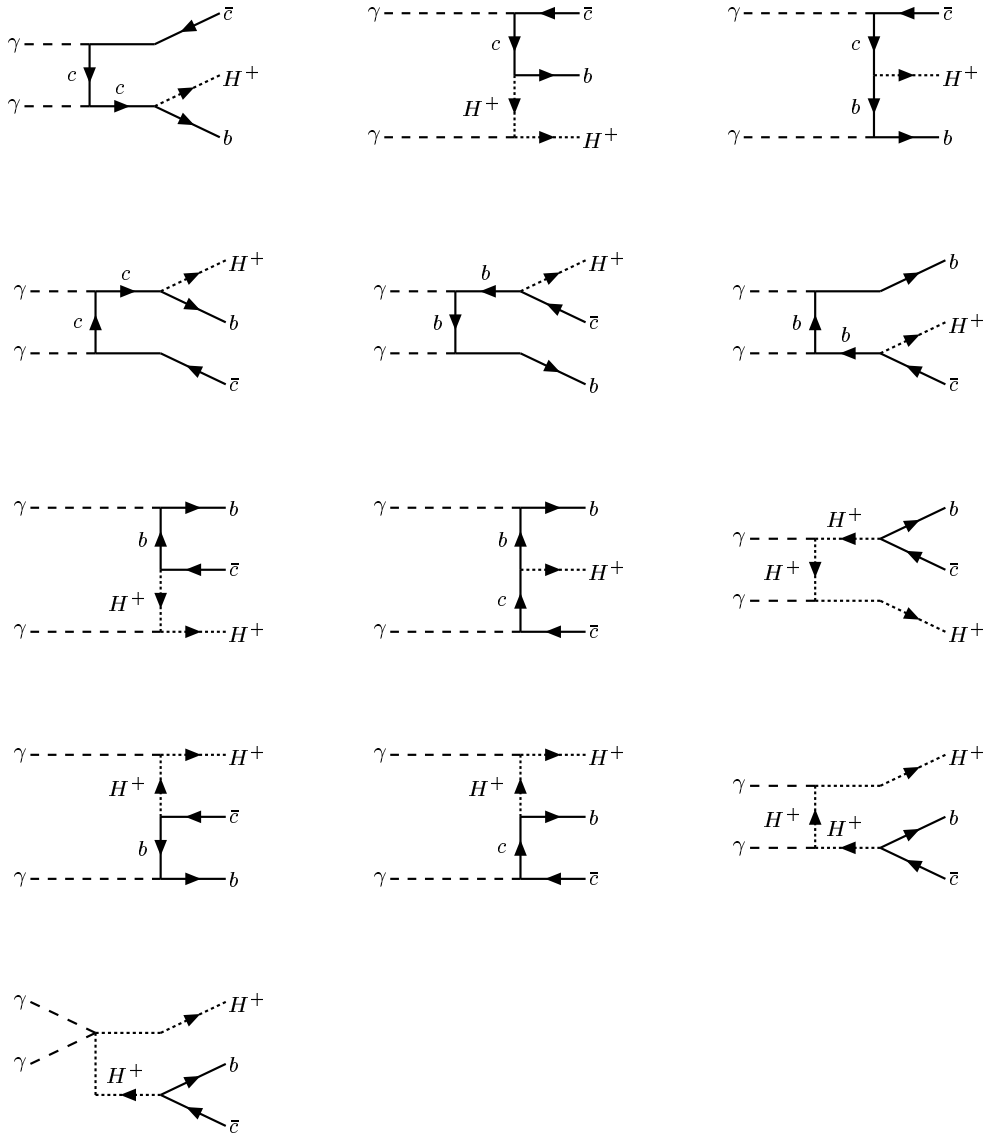


FIG. 5: The complete set of Feynman diagrams for  $\gamma\gamma \rightarrow b\bar{c}H^+$ .

becomes available. Furthermore, for  $M_{H^\pm} < \sqrt{s}/2$ , the cross section in  $\gamma\gamma$  collisions is typically an order of magnitude larger than that in  $e^-e^+$  collisions.

It is evident that the cross section of  $\gamma\gamma \rightarrow b\bar{c}H^+$  is larger than that of  $e^+e^- \rightarrow b\bar{c}H^+$  in the whole  $M_{H^\pm}$  region. For  $M_{H^\pm} > \sqrt{s}/2$ , where the pair production is not kinematically allowed, the difference between these two cross sections becomes much larger (two to three

orders of magnitude) for a larger  $M_{H^\pm}$  value. To understand the cause of this difference, we have to examine the Feynman diagrams that contribute to the scattering processes  $e^-e^+ \rightarrow b\bar{c}H^+$  and  $\gamma\gamma \rightarrow b\bar{c}H^+$ . The complete set of Feynman diagrams for the above processes are depicted in Figs. 4 and 5, respectively. In the former process, all the Feynman diagrams contain an  $s$ -channel propagator which is either a virtual photon or a virtual  $Z$  boson. Therefore, when  $M_{H^\pm}$  increases for a fixed  $\sqrt{s}$ , the cross section decreases rapidly. On the contrary, in the latter process, when  $M_{H^\pm} > \sqrt{s}/2$ , the dominant contribution arises from the fusion diagram  $\gamma\gamma \rightarrow (c\bar{c})(b\bar{b}) \rightarrow b\bar{c}H^+$ , whose contribution is enhanced by the two collinear poles (in a  $t$ -channel diagram) generated from  $\gamma \rightarrow c\bar{c}$  and  $\gamma \rightarrow b\bar{b}$  in high energy collisions. Since the collinear enhancement takes the form of  $\ln(M_{H^\pm}/m_q)$ , with  $m_q$  being the bottom or charm quark mass, the cross section of  $\gamma\gamma \rightarrow b\bar{c}H^+$  does not vary much as  $M_{H^\pm}$  increases until it is close to  $\sqrt{s}$ .

From the above discussions we conclude that a photon-photon collider is superior to an electron-positron collider for detecting a heavy charged Higgs boson. Moreover, a polarized photon collider can determine the chirality structure of the fermion Yukawa couplings with the charged Higgs boson via single charged Higgs production. This point is illustrated as follows. First, let us consider the case that  $M_{H^\pm} > \sqrt{s}/2$ . As noted above, in this case, the production cross section is dominated by the fusion diagram  $\gamma\gamma \rightarrow (c\bar{c})(b\bar{b}) \rightarrow b\bar{c}H^+$ . In the TopC model, because  $Y_L^{bc} = 0$  (and  $Y_R^{bc} \neq 0$ ), it corresponds to  $\gamma\gamma \rightarrow (c_R\bar{c}_R)(b_L\bar{b}_L) \rightarrow b_L\bar{c}_R H^+$ . On the other hand, in the MSSM with stop-scharm mixings and large  $\tan\beta$ ,  $Y_R^{bc} \sim 0$  (and  $Y_L^{bc} \neq 0$ ), it becomes  $\gamma\gamma \rightarrow (c_L\bar{c}_L)(b_R\bar{b}_R) \rightarrow b_R\bar{c}_L H^+$ . Therefore, we expect that if both photon beams are right-handedly polarized (i.e.  $\gamma_R\gamma_R$ ), then a TopC charged Higgs boson (i.e. top-pion) can be copiously produced, while a MSSM charged Higgs boson (with a large  $\tan\beta$ ) is highly suppressed. To detect a MSSM charged Higgs boson, both photon beams have to be left-handedly polarized (i.e.  $\gamma_L\gamma_L$ ). This is supported by an exact

calculation whose results are shown in Figs. 8 and 9 for the TopC model at two different collider energies. A similar feature also holds for the MSSM after interchanging the label of  $RR$  and  $LL$  in those figures, which can be verified in Figs. 10 and 11.

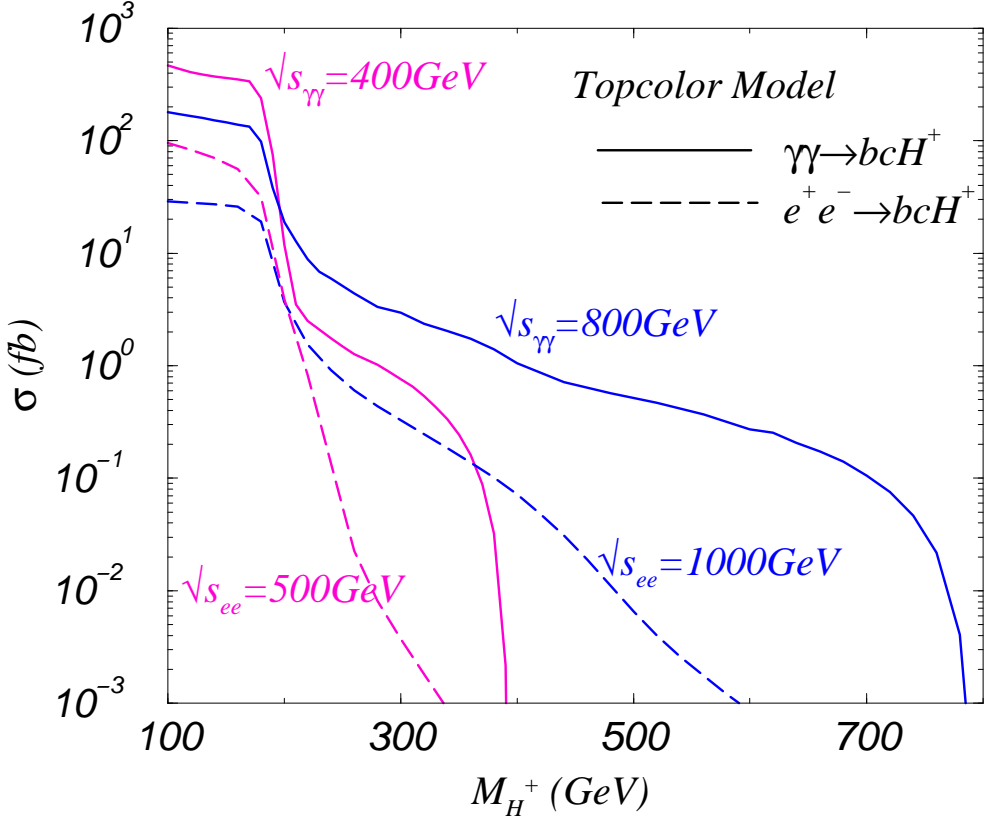


FIG. 6: Cross sections of  $\gamma\gamma \rightarrow b\bar{c}H^+$  (solid curve) and  $e^+e^- \rightarrow b\bar{c}H^+$  (dashed curve) for the TopC model [cf. Eq. (15)] with unpolarized photon beams at  $\sqrt{s} = 400$  GeV and 800 GeV.

The feature of the polarized photon cross sections for  $M_{H^\pm} < \sqrt{s}/2$  can be understood from examining the production process  $\gamma\gamma \rightarrow H^+H^-$ . The helicity amplitudes for the  $H^+H^-$  pair production in polarized photon collisions can be computed as

$$M(\gamma_{\lambda_1}\gamma_{\lambda_2} \rightarrow H^+H^-) = 2e^2\lambda_1\lambda_2 \frac{1-\xi^2}{1-\xi^2\cos^2\Theta} + e^2(1-\lambda_1\lambda_2), \quad (16)$$

where the degree of polarization of the initial state photons,  $\lambda_1$  and  $\lambda_2$ , can take the value

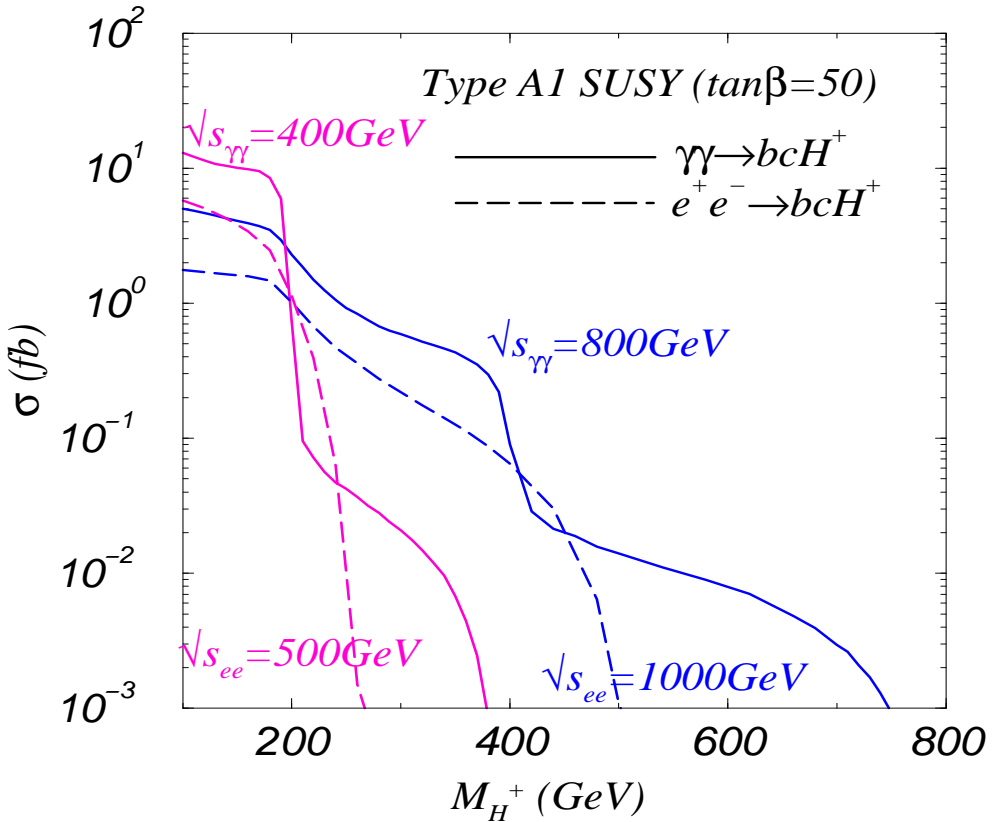


FIG. 7: Same as Fig. 6, but for the MSSM with stop-scharm mixings, i.e. Type-A SUSY model [cf. Eq. (11)].

of either  $-1$  or  $+1$ , corresponding to a left-handedly ( $L$ ) and right-handedly ( $R$ ) polarized photon beam, respectively;  $\Theta$  is the scattering angle of  $H^+$  in the center-of-mass frame; and  $\xi = \sqrt{1 - 4M_{H^\pm}^2/s}$ . In the massless limit, i.e., when  $M_{H^\pm} \rightarrow 0$ , the above result reduces to  $M(\gamma_{\lambda_1}\gamma_{\lambda_2} \rightarrow H^+H^-) \simeq e^2(1 - \lambda_1\lambda_2)$ . Let us denote  $\sigma_{\lambda_1\lambda_2}^{\text{pair}}$  as the cross section of  $\gamma_{\lambda_1}\gamma_{\lambda_2} \rightarrow H^+H^-$ . We find that  $\sigma_{LR}^{\text{pair}} = \sigma_{RL}^{\text{pair}}$ , and they dominate the total cross section when  $M_{H^\pm}^2 \ll s$ , while  $\sigma_{LL}^{\text{pair}}$  and  $\sigma_{RR}^{\text{pair}}$  are equal and approach zero as  $M_{H^\pm} \rightarrow 0$ . Since for  $M_{H^\pm} < \sqrt{s}/2$  the bulk part of the cross section of  $\gamma\gamma \rightarrow b\bar{c}H^+$  comes from  $\sigma(\gamma\gamma \rightarrow H^+H^-) \times \text{Br}(H^- \rightarrow b\bar{c})$ , the  $LL$  and  $RR$  cross sections are smaller than the  $LR$  ( $= RL$ ) cross sections as  $M_{H^\pm}$  decreases, cf. Fig. 8.

It is important to point out that the complete set of Feynman diagrams have to be included to calculate  $\sigma(\gamma\gamma \rightarrow b\bar{c}H^+)$  even when  $M_{H^\pm} < \sqrt{s}/2$  because of the requirement of gauge invariance. To study the effect of the additional Feynman diagrams, other than those contributing to the  $H^+H^-$  pair production from  $\gamma\gamma \rightarrow H^+H^- (\rightarrow b\bar{c})$ , one can examine the *single* charged Higgs boson rate in this regime with the requirement that the invariant mass of  $b\bar{c}$ , denoted as  $M_{b\bar{c}}$ , satisfies the following condition:

$$\begin{aligned} |M_{b\bar{c}} - M_{H^\pm}| &> \Delta M_{b\bar{c}}, \quad \text{with} \\ \Delta M_{b\bar{c}} &= \min \left[ 25 \text{ GeV}, \max \left[ 1.18 M_{c\bar{b}} \frac{2\delta m}{m}, \Gamma_{H^+} \right] \right], \\ \frac{\delta m}{m} &= \frac{0.5}{\sqrt{M_{b\bar{c}}/2}}, \end{aligned} \quad (17)$$

where  $\frac{\delta m}{m}$  denotes the mass resolution of the detector for observing the final state  $b$  and  $\bar{c}$  jets originated from the decay of  $H^-$ . For instance, in Fig. 8 the set of dashed-lines are the polarized cross sections after imposing the above kinematical cut. With this cut, the total rate reduces by about one order of magnitude for  $M_{H^\pm} < \sqrt{s}/2$ . (However, this kinematical cut hardly changes the event rate when  $M_{H^\pm} > \sqrt{s}/2$ .) The effect of this kinematic cut on the  $RR$  and  $LL$  rates are significantly different in the low  $M_{H^\pm}$  region. It implies that the  $H^+H^-$  pair production diagrams cannot be the whole production mechanism, otherwise, we would expect the rates of  $RR$  and  $LL$  to be always equal due to the parity invariance of the QED theory. Again, a similar feature also holds for the MSSM after interchanging the labels of  $LL$  and  $RR$ .

Before closing this section, we remark that in the MSSM a heavy charged Higgs boson  $H^+$  can also be produced associated with a  $\bar{c}s$  pair, whose production rate can be obtained by rescaling the cross sections in Fig. 7 by the factor

$$\left( Y_{L(0)}^{sc} / Y_L^{bc} \right)^2 = 1.3 (\tan \beta)^2 \times 10^{-4}$$

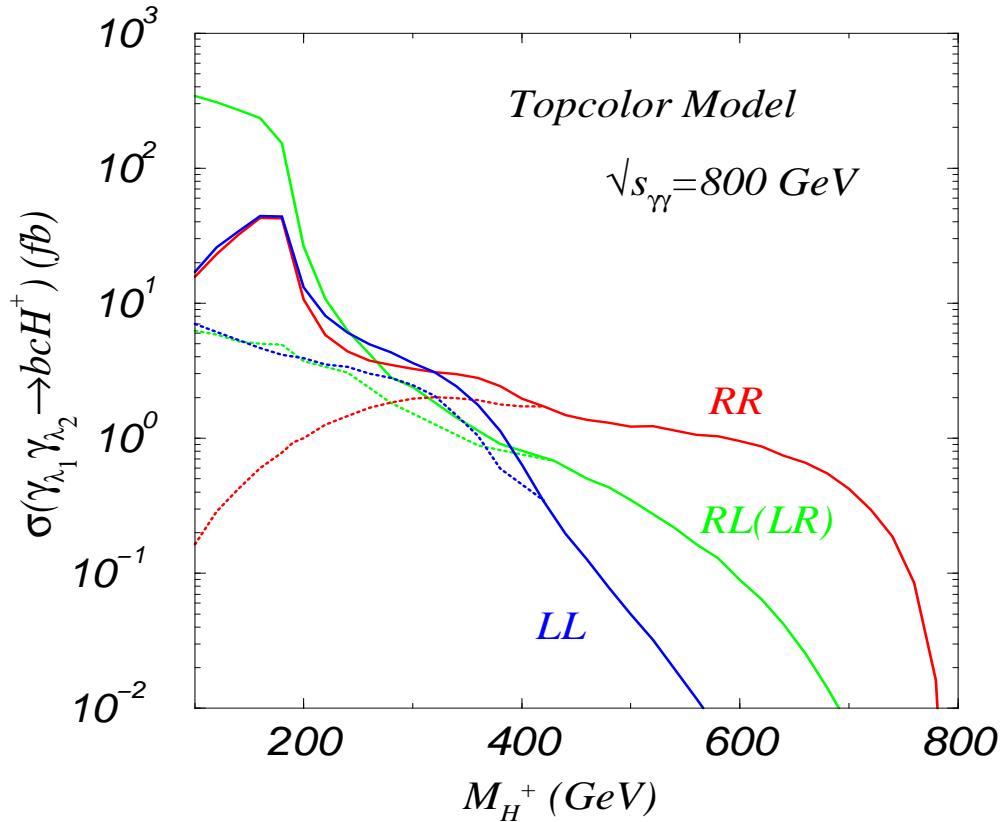


FIG. 8: Cross sections of  $\gamma_{\lambda_1}\gamma_{\lambda_2} \rightarrow b\bar{c}H^+$  at  $\sqrt{s} = 800$  GeV in polarized photon collisions for the TopC model [cf. Eq. (15)]. Solid curves are the results without any kinematical cut, and Dashed curves are the results with the kinematical cut specified in the text [cf. Eq. (17)].

for  $M_{H^\pm} > \sqrt{s}/2$ . Here,  $Y_{L(0)}^{sc} = \frac{\sqrt{2}m_s}{v} \tan \beta$ , and the running mass of the strange quark at the scale of 100 GeV is taken to be  $m_s \simeq 0.1$  GeV. Hence, for  $\tan \beta = 30$ , the production rate of  $scH^\pm$  is down by a factor of 100.

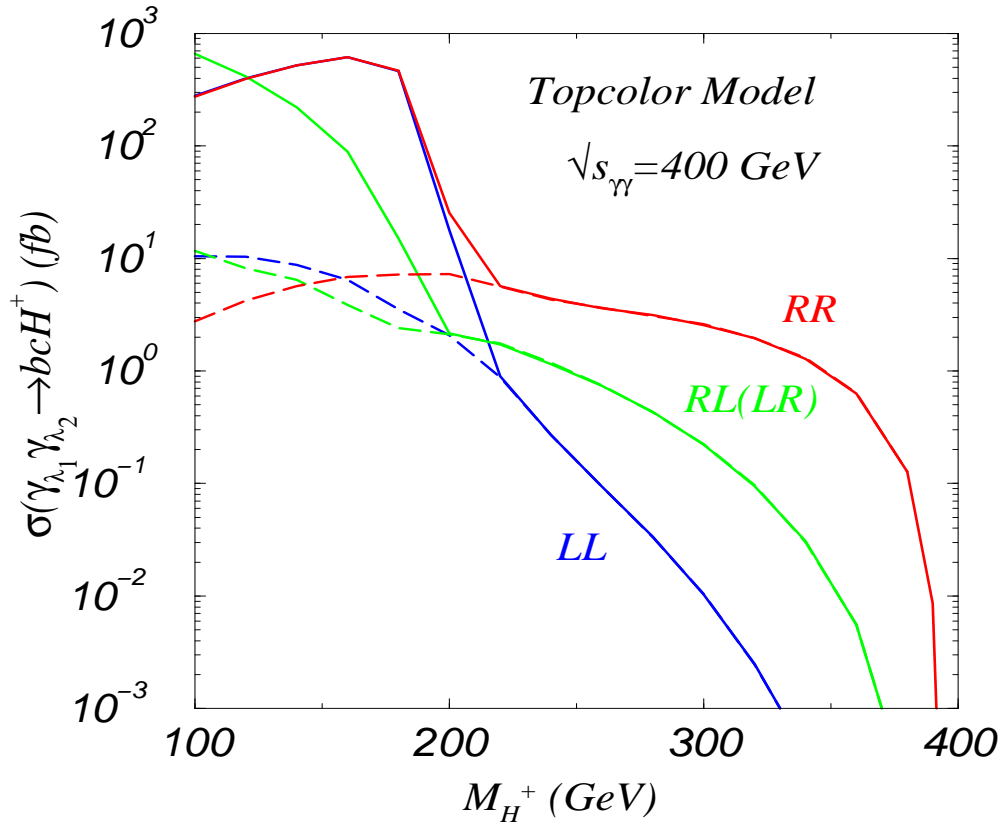


FIG. 9: Same as Fig. 8, but for  $\sqrt{s} = 400$  GeV.

### B. $\tau\nu H^\pm$ Production

In the MSSM with a large  $\tan\beta$  value, the cross section of  $\gamma\gamma \rightarrow \tau^-\bar{\nu}H^+$  can be quite sizable. For the sample parameters chosen in Eq. (3), its cross sections are shown in Fig. 12 for various linear colliders with unpolarized collider beams. (Our results are consistent with the calculation in Refs. [28, 29].) Recall that we have chosen the sample parameters of the models so that the Yukawa coupling of  $\tau$ - $\nu$ - $H^+$  in the MSSM and that of  $b$ - $c$ - $H^+$  in the TopC model have the same magnitude but opposite chiralities, as shown in Eqs. (3) and (15). The gross feature of this figure is similar to Fig. 8. However, a close examination reveals that the cross section of  $\gamma\gamma \rightarrow \tau^-\bar{\nu}H^+$  is smaller than that of  $\gamma\gamma \rightarrow b\bar{c}H^+$  at a fixed  $M_{H^\pm}$  for

$M_{H^\pm} > \sqrt{s}/2$ . For instance, for a 700 GeV charged Higgs boson,  $\sigma(\gamma\gamma \rightarrow \tau^-\bar{\nu}H^+) \sim 0.02 \text{ fb}$  and  $\sigma(\gamma\gamma \rightarrow b\bar{c}H^+) \sim 0.3 \text{ fb}$ . This difference can again be understood by examining the Feynman diagrams. In the scattering  $\gamma\gamma \rightarrow b\bar{c}H^+$ , the total cross section is dominated by the fusion diagram  $\gamma\gamma \rightarrow (c\bar{c})(b\bar{b}) \rightarrow b\bar{c}H^+$  for  $M_{H^\pm} > \sqrt{s}/2$ . The contribution of this diagram is enhanced by two collinear poles (in a  $t$ -channel diagram) generated from  $\gamma \rightarrow c\bar{c}$  and  $\gamma \rightarrow b\bar{b}$  in high energy collisions. However, in the scattering  $\gamma\gamma \rightarrow \tau^-\bar{\nu}H^+$ , the dominant contribution in the large mass region comes from the sub-diagram  $\gamma\tau_R \rightarrow H^+\bar{\nu}_L$ , and contains only one collinear pole (in a  $t$ -channel diagram) generated from  $\gamma \rightarrow \tau\bar{\tau}$  in high energy collisions. This is because photon does not couple to neutrinos. Hence, the production rate of  $\tau\nu H^+$  is not as large as that of  $b\bar{c}H^+$ , even when the relevant Yukawa couplings are of the same magnitude in both production channels.

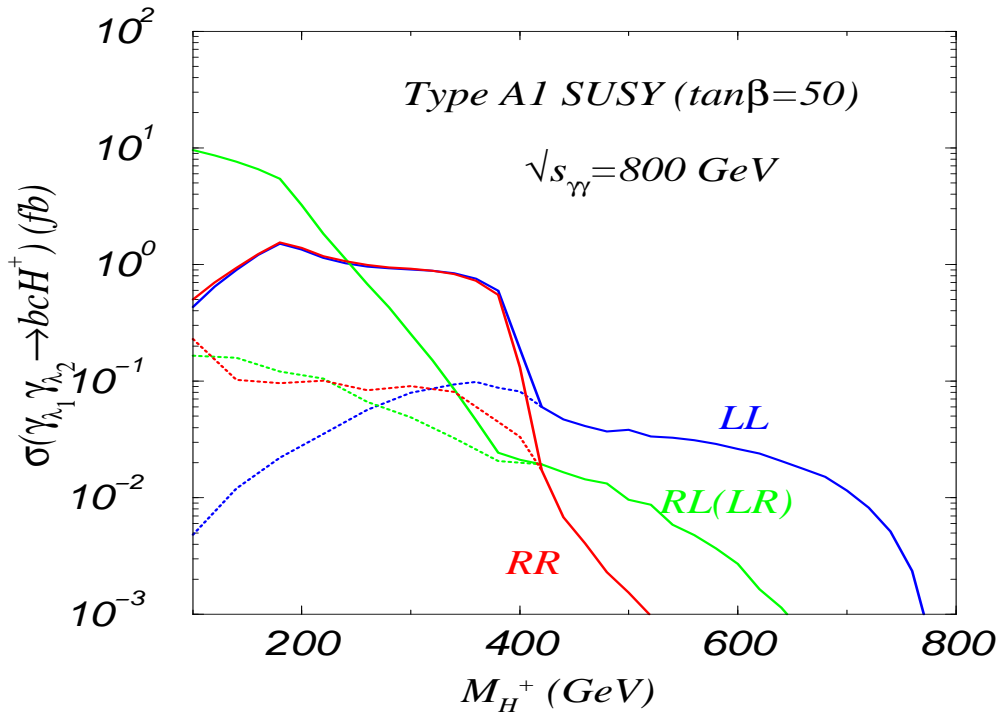


FIG. 10: Cross sections of  $\gamma\lambda_1\gamma\lambda_2 \rightarrow b\bar{c}H^+$  at  $\sqrt{s} = 800 \text{ GeV}$  in polarized photon collisions for the Type-A SUSY model [cf. Eq. (11)]. Solid curves are the results without any kinematical cut, and Dashed curves are the results with the kinematical cut specified in the text [cf. Eq. (17)].

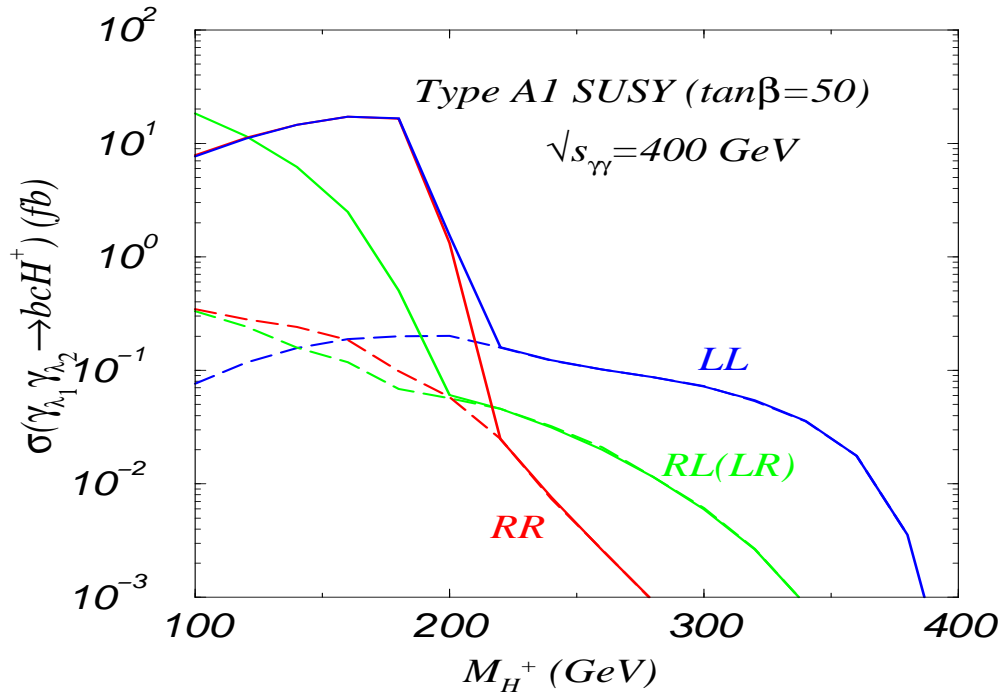


FIG. 11: Same as Fig. 10, but for  $\sqrt{s} = 400$  GeV.

We also computed the production cross section  $\sigma(\gamma_{\lambda_1}\gamma_{\lambda_2} \rightarrow \tau\nu H^+)$  in the polarized photon-photon collisions, and the results are shown in Figs. 13 and 14. As expected, *LL* rate is the dominant one when  $M_{H^\pm} > \sqrt{s}/2$ , because the Yukawa couplings  $Y_R^{\tau\nu} = 0$  and  $Y_L^{\tau\nu} \neq 0$ . The *single* charged Higgs boson production rate for  $M_{H^\pm} < \sqrt{s}/2$  is also calculated by imposing the kinematical cut:

$$\begin{aligned}
 |M_{\tau\bar{\nu}} - M_{H^\pm}| &> \Delta M_{\tau\bar{\nu}}, \quad \text{with} \\
 \Delta M_{\tau\bar{\nu}} &= \min \left[ 25 \text{ GeV}, \max \left[ 1.18 M_{\tau\bar{\nu}} \frac{2\delta m}{m}, \Gamma_{H^+} \right] \right], \\
 \frac{\delta m}{m} &= \frac{0.5}{\sqrt{M_{\tau\bar{\nu}}/2}}, \tag{18}
 \end{aligned}$$

and the result is shown in Figs. 13 and 14. (In reality,  $M_{\tau\bar{\nu}}$  should be replaced by, for instance, the transverse mass of the  $\tau\bar{\nu}$  pair.) For our choice of parameters in Eq. (3),  $\Gamma_{H^+}$  is about 0.54 GeV (4.7 GeV) for a Higgs mass 200 GeV (400 GeV), and correspondingly,  $\text{Br}(H^- \rightarrow \tau^-\bar{\nu})$  is about 0.69 (0.16).

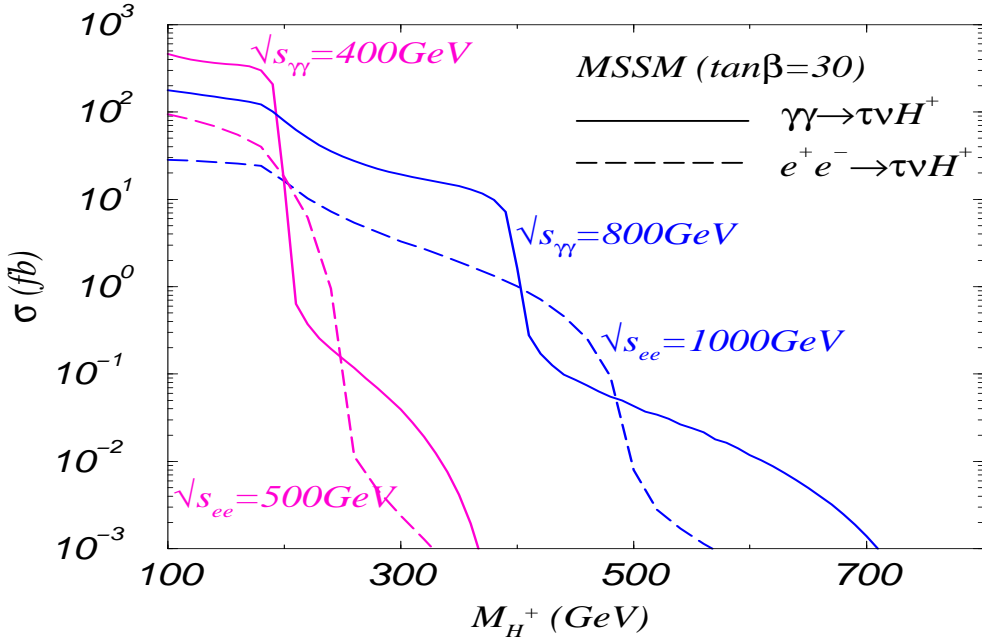


FIG. 12: Cross sections of  $\gamma\gamma \rightarrow \tau^-\bar{\nu}H^+$  (solid curve) and  $e^+e^- \rightarrow \tau\bar{\nu}H^+$  (dashed curve) for the MSSM [cf. Eq. (3)] with unpolarized beams at  $\sqrt{s} = 400$  GeV and 800 GeV.

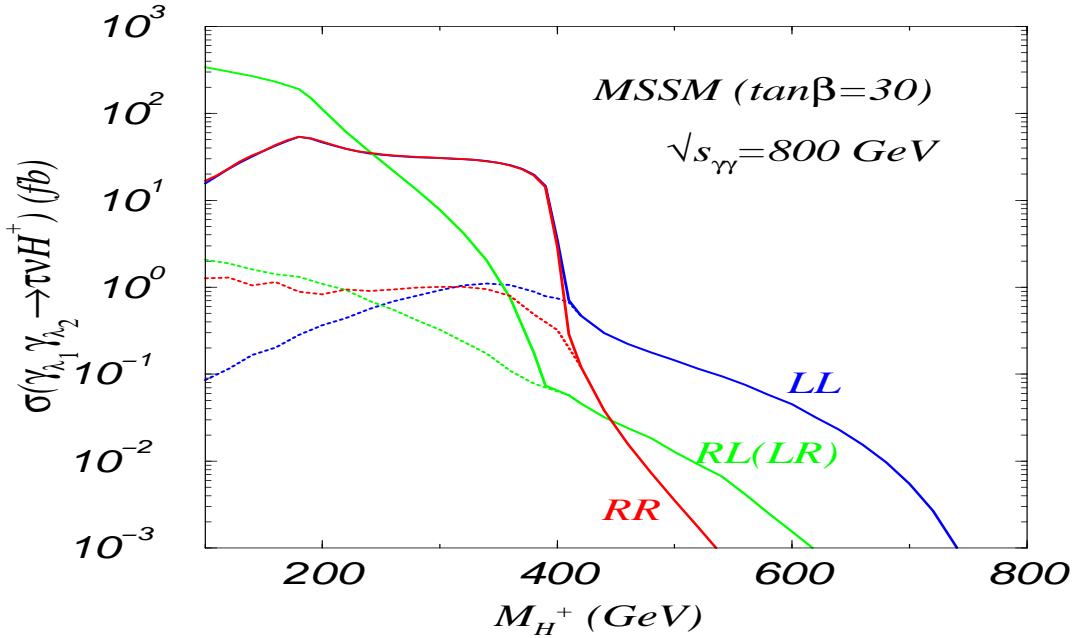


FIG. 13: Cross sections of  $\gamma_{\lambda_1}\gamma_{\lambda_2} \rightarrow \tau\bar{\nu}H^+$  at  $\sqrt{s} = 800$  GeV in polarized photon collisions for the MSSM [cf. Eq. (3)]. Solid curves are the results without any kinematical cut, and Dashed curves are the results with the kinematical cut specified in the text [cf. Eq. (18)].

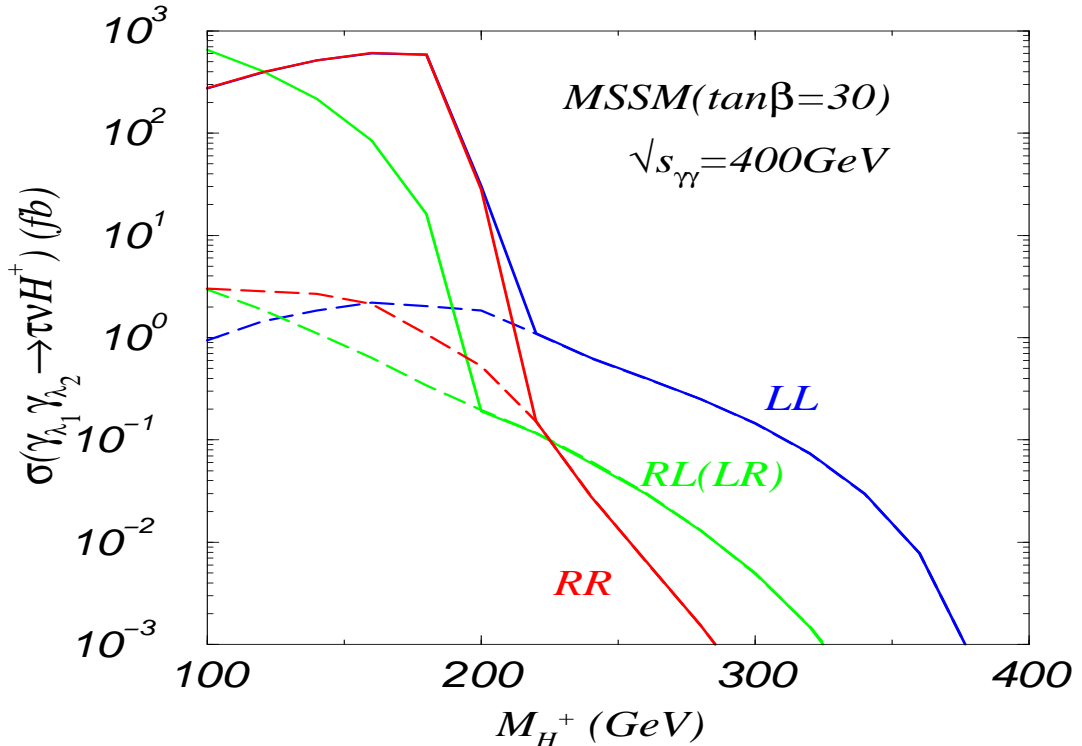


FIG. 14: Same as Fig. 13, but for  $\sqrt{s} = 400$  GeV.

#### IV. CONCLUSIONS

In this work, we have studied the single charged scalar production at polarized photon colliders via the fusion processes  $\gamma\gamma \rightarrow b\bar{c}H^+$  and  $\gamma\gamma \rightarrow \tau\bar{\nu}H^+$ . For the  $b\bar{c}H^+$  production, we consider the flavor mixing couplings of  $b$ - $c$ - $H^\pm$  generated from the natural stop-scharm mixings in the MSSM, and from the generic mixings of the right-handed top and charm quarks in the dynamical Top-color model. For the  $\tau\bar{\nu}H^+$  production, we consider the MSSM with a moderate to large  $\tan\beta$ . We find that the production rate of  $H^+$  in the  $\gamma\gamma$  collisions is much larger than that in the  $e^-e^+$  collision. (Needless to say that the production rate of  $H^-$  is the same as  $H^+$ .) Some of the results are shown in Figs. 6, 7 and 12. For  $M_{H^+} > \sqrt{s}/2$ , the cross section of  $\gamma\gamma \rightarrow \tau\bar{\nu}H^+$  is smaller than that of  $\gamma\gamma \rightarrow b\bar{c}H^+$  even when the corresponding Yukawa couplings are of the same size. This is because in high energy collisions

there is only one collinear pole [ $\gamma\gamma \rightarrow (\tau\bar{\tau})\gamma \rightarrow \tau\bar{\nu}H^+$ ] in the scattering  $\gamma\gamma \rightarrow \tau\bar{\nu}H^+$ , but two collinear poles [ $\gamma\gamma \rightarrow (c\bar{c})(b\bar{b}) \rightarrow b\bar{c}H^+$ ] in  $\gamma\gamma \rightarrow b\bar{c}H^+$ . The same reason also explains why in the large  $M_{H^+}$  region the  $e^+e^-$  rate is smaller than the  $\gamma\gamma$  rate by at least one to two orders of magnitude, since the  $e^+e^-$  processes contain only *s*-channel diagrams and cannot generate any collinear enhancement factor to the single charged Higgs boson production rate. Furthermore, we show that it is possible to measure the Yukawa couplings  $Y_L$  and  $Y_R$ , separately, at photon-photon colliders by properly choosing the polarization states of the incoming photon beams. This unique feature of the photon colliders can be used to discriminate new dynamics of the flavor symmetry breaking.

Given our results of the cross sections, it is trivial to deduce the signal event rates as long as the integrated luminosity of the collider is known. According to the reports of the LC Working Groups in Refs. [30] and [31], the integrated luminosity can reach about  $500\text{ fb}^{-1}$  at a 500 GeV LC, and  $1000\text{ fb}^{-1}$  at an 1 TeV LC. Hence, we conclude that a polarized photon-photon collider is not only useful for determining the  $\text{CP}$  property of a neutral Higgs boson, but also important for detecting a heavy charged Higgs boson and determining the chirality structure of the corresponding fermion Yukawa interactions with the charged Higgs boson.

### Acknowledgments

We thank Gordon L. Kane for valuable discussions on the SUSY flavor mixings. SK would like to thank Stefano Moretti for useful discussions and for comparing part of our results with his calculation. This work was supported in part by the NSF grant PHY-0100677 and DOE grant DEFG0393ER40757.

## References

---

- [1] P. W. Higgs, Phys. Lett. **B12**, 132 (1964); Phys. Rev. Lett. **13**, 508 (1964); Phys. Rev. **145**, 1156 (1966); F. Englert and R. Brout, Phys. Rev. Lett. **13**, 321 (1964); G. S. Guralnik, C. R. Hagen, and T. W. Kibble, Phys. Rev. Lett. **13**, 585 (1964).
- [2] P. Fayet and S. Ferrara, Phys. Rept. **32**, 249 (1977); H. P. Nilles, Phys. Rept. **110**, 1 (1984); H. E. Haber and G. L. Kane, Phys. Rept. **117**, 75 (1985); and reviews in “Perspectives on Supersymmetry”, ed. G. L. Kane, World Scientific Publishing Co., 1998.
- [3] For an updated comprehensive review of the dynamical symmetry breaking and compositeness, C. T. Hill and E. H. Simmons, [hep-ph/0203079](#).
- [4] For recent reviews of MSSM, see, *e.g.*, H. E. Haber, Nucl. Phys. Proc. Suppl. **101**, 217 (2001) [[hep-ph/0103095](#)]; and G. L. Kane, *Lectures at the Latin American School, SILAAE III* [[hep-ph/0008190](#)].
- [5] C. T. Hill, Phys. Lett. **B345**, 483 (1995) [[hep-ph/9411426](#)]; and Phys. Lett. **B266**, 419 (1991).
- [6] F. Bolzumati, in  $e^+e^-$  Collisions at 500 GeV, ed. P. M. Zerwas, DESY 93-099, p.261-268, [hep-ph/9310348](#); J. A. Coarasa, J. Guasch, J. Sola and W. Hollik, Phys. Lett. B **442**, 326 (1998) [[hep-ph/9808278](#)]; J. A. Coarasa, D. Garcia, J. Guasch, R. A. Jimenez and J. Sola, Euro. Phys. J. C **2**, 373 (1998) [[hep-ph/9607485](#)].
- [7] J. Gunion, G. Ladinsky, C.-P. Yuan, *et al.*, in *Proceedings of Snowmass Summer Study*, pp. 59-81, Snowmass, Colorado, 1990 (World Scientific, Singapore, 1992); V. Barger, R. J. N. Phillip and D. P. Roy, Phys. Lett. B **324**, 236 (1994) [[hep-ph/9311372](#)]; F. Borzumati, J. Kneur, N. Polonsky, Phys. Rev. D **60**, 115011 (1999) [[hep-ph/9905443](#)]; A. Belyaev, D. Garcia, J. Guasch, J. Solà, JHEP **0206**, 059 (2002) [[hep-ph/0203031](#)].
- [8] H.-J. He and C.-P. Yuan, Phys. Rev. Lett. **83**, 28 (1999) [[hep-ph/9810367](#)].
- [9] C. Balazs, H.-J. He, C.-P. Yuan, Phys. Rev. D **60**, 114001 (1999) [[hep-ph/9812263](#)].
- [10] J.L. Diaz-Cruz, H.-J. He, C.-P. Yuan, Phys. Lett. B **530**, 179 (2002) [[hep-ph/0103178](#)].
- [11] For a recent application to the LHC-CMS analysis, S. R. Slabospitsky, CMS-Note-2002/010, [[hep-ph/0203094](#)].

- [12] A.A. Barrientos Bendezu and B. A. Kniehl, Phys. Rev. D **59**, 015009 (1999) [[hep-ph/9807480](#)], Phys. Rev. D **61**, 097701 (2000) [[hep-ph/9909502](#)], Phys. Rev. D **63**, 015009 (2001) [[hep-ph/0007336](#)]; O. Brein, W. Hollik and S. Kanemura, Phys. Rev. D **63**, 095001 (2001) [[hep-ph/0008308](#)].
- [13] S. Moretti and K. Odagiri, Phys. Rev. D **59**, 055008 (1999) [[hep-ph/9809244](#)].
- [14] A. A. Barrientos Bendezu and B. A. Kniehl, Nucl. Phys. B **568**, 305 (2000) [[hep-ph/9908385](#)]; O. Brein and W. Hollik, Euro. Phys. J. C **13**, 175 (2000) [[hep-ph/9908529](#)].
- [15] S. Komamiya, Phys. Rev. D **38**, 2158 (1988).
- [16] S.-H. Zhu, [hep-ph/9901221](#); S. Kanemura, Euro. Phys. J. C **17**, 473 (2000) [[hep-ph/9911541](#)], A. Arhrib, M. Capdequi Peyranere, W. Hollik and G. Moultsaka, Nucl. Phys. B **581**, 34 (2000) [[hep-ph/9912527](#)], H. E. Logan, S. Su, Phys. Rev. D **66**, 035001 (2002) [[hep-ph/0203270](#)].
- [17] S. Kanemura, S. Moretti and K. Odagiri, JHEP **0102**, 011 (2001) [[hep-ph/0012020](#)], S. Kanemura, S. Moretti and K. Odagiri, Proceedings of Linear Collider Workshop 2000 at Fermilab [[hep-ph/0012020](#)].
- [18] H.-J. He, S. Kanemura, C.-P. Yuan, Phys. Rev. Lett. **89**, 101803 (2002) [[hep-ph/0203090](#)].
- [19] B. Grazadkowski and J. F. Gunion, Phys. Lett. B **294**, 361 (1992) [[hep-ph/9206262](#)].
- [20] E. Asakawa, S. Y. Choi, K. Hagiwara and J.-S. Lee, Phys. Rev. D **62**, 115005 (2000) [[hep-ph/0005313](#)].
- [21] For reviews, M. S. Chanowitz, Nucl. Instr. & Meth. A **355**, 42 (1995); H. Murayama and M. E. Peskin, Ann. Rev. Nucl. Part. Sci. **46**, 533 (1996) [[hep-ex/9606003](#)]; E. Accomando *et al.*, Phys. Rept. **299**, 1 (1998) [[hep-ph/9705542](#)].
- [22] J. A. Casas and S. Dimopolous, Phys. Lett. B **387**, 107 (1996) [[hep-ph/9606237](#)].
- [23] M. Misiak, S. Pokorski, J. Rosiek, “Supersymmetry and FCNC Effects”, [hep-ph/9703442](#), in *Heavy Flavor II*, pp. 795, eds., A. J. Buras and M. Lindner, Advanced Series on Directions in High Energy Physics, World Scientific Publishing Co., 1998, and references therein.
- [24] C. Balazs, J.L. Diaz-Cruz, H.-J. He, T. Tait, C.-P. Yuan, Phys. Rev. D **59**, 055016 (1999) [[hep-ph/9807349](#)].
- [25] M. Carena, S. Mrenna, C.E.M. Wagner, Phys. Rev. D **60**, 075010 (1999) [[hep-ph/9808312](#)].
- [26] R. Hempfling, Phys. Rev. D **49**, 6168 (1994); L. J. Hall, R. Rattazzi, U. Sarid, Phys. Rev. D

**50**, 7048 (1994) [[hep-ph/9306309](#)]; M. Carena, M. Olechowski, S. Pokorski, C.E.M. Wagner, Nucl. Phys. B **426**, 269 (1994) [[hep-ph/9402253](#)].

[27] M. Capdequi Peylanere, H. E. Haber and P. Irulegui, Phys. Rev. D **44**, 191 (1991); A. Mendez and A. Pomarol, Nucl. Phys. B **349**, 369 (1991); S. Kanemura, Phys. Rev. D **61**, 095001 (2000) [[hep-ph/9710237](#)].

[28] S. Kanemura, S. Moretti and K. Odagiri, in preparation.

[29] S. Moretti, talk at the International Workshop on Linear Colliders (LCWS2002), Korea, August 26-30, 2002 [[hep-ph/0209210](#)].

[30] ECFA/DESY Linear Collider Physics Working Group, TESLA Technical Design Report Part III: “*Physics at an  $e^+e^-$  Linear Collider*” [[hep-ph/0106315](#)].

[31] ACFA Linear Collider Physics Working Group, “*Particle Physics Experiment at JLC*” [[hep-ph/0109166](#)].

[32] The electroweak gauge contribution depends also on other supersymmetry (SUSY) parameters [26]. Here,  $M_2$  is taken to be 300 GeV, but higher values of  $M_2$  will make the electroweak gauge contribution even smaller due to the decoupling feature.